**Title**
Battery aging in multi-energy microgrid design using mixed integer linear programming



**Authors**
Cardoso, Gonçalo
Brouhard, Thomas
DeForest, Nicholas
et al.

**Publication Date**
2018-12-01

**DOI**
10.1016/j.apenergy.2018.09.185

Peer reviewed

LBNL-0000

# Lawrence Berkeley National Laboratory

# Battery aging in multi-energy microgrid design using mixed integer linear programming

G. Cardoso[a], T. Brouhard[b], N. DeForest[a], D. Wang[a], M. Heleno[a], L. Kotzur[a,c]

[a] Lawrence Berkeley National Laboratory, University of California, 1 Cyclotron Rd, Berkeley, CA, USA
[b] Mines ParisTech, 60, Boulevard Saint-Michel 75 272 PARIS cedex 06
[c] Institute of Electrochemical Process Engineering (IEK-3), Forschungszentrum Julich GmbH, Wilhelm-Johnen-Str., 52428 Julich, Germany

**Published in Applied Energy**

**December 2018**

Partial funding for this work was provided by the Office of Electricity, Microgrids R&D and Advanced Grid Modeling Programs, of the U.S. Department of Energy under Contract No. DE-AC02-05CH11231.

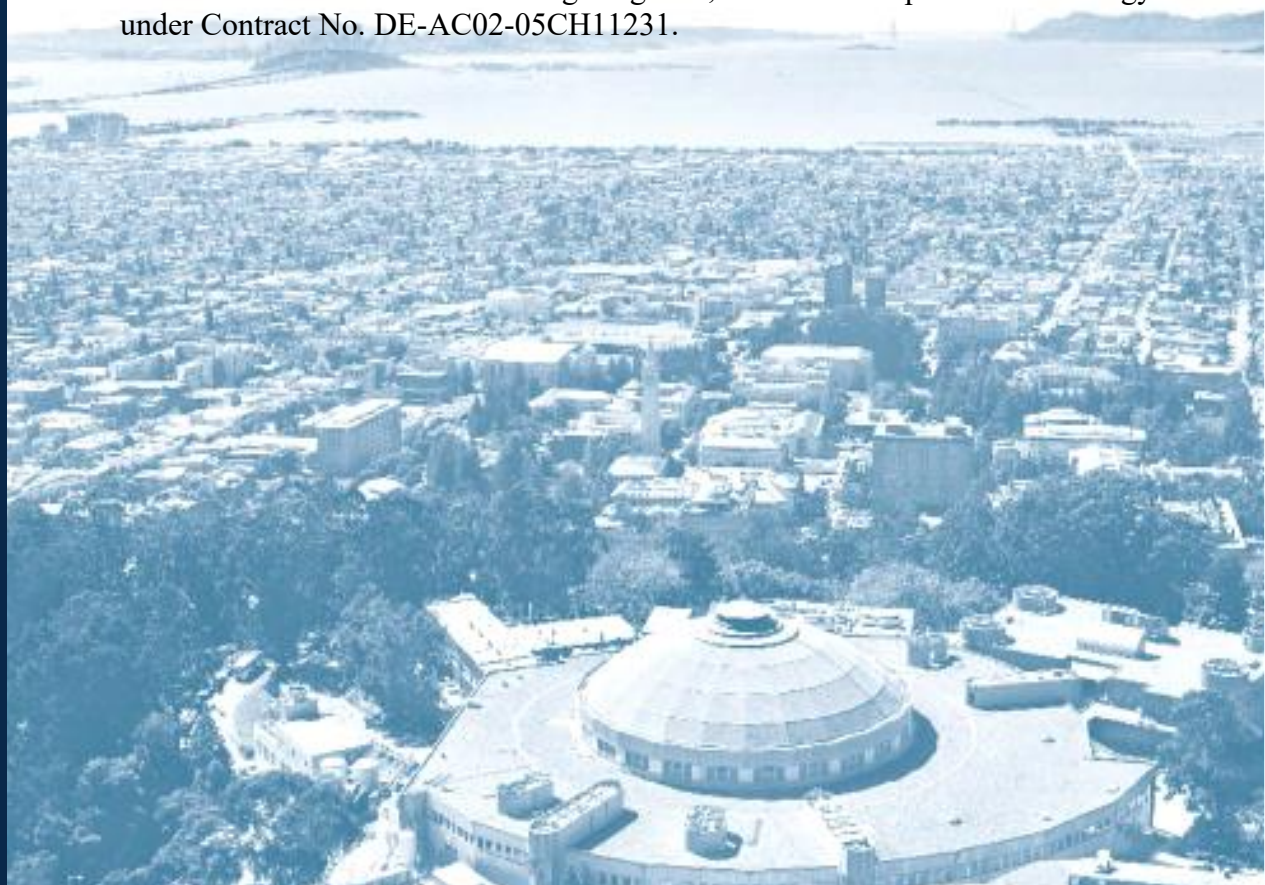

# Disclaimer

**Manuscript for *Applied Energy - Distributed Energy & Microgrids Special Issue***

# Battery aging in multi-energy microgrid design using mixed integer linear programming

Gonçalo Cardoso[1*]
Email: gfcardoso@lbl.gov

Thomas Brouhard[1,2]
Email: thomas.brouhard@mines-paristech.fr

Nicholas DeForest[1]
Email: ndeforest@lbl.gov

Dai Wang[1]
Email: daiwang@lbl.gov

Miguel Heleno[1]
Email: miguelheleno@lbl.gov

Leander Kotzur[1,3]
Email: l.kotzur@fz-juelich.de

1. Grid Integration Group
   Lawrence Berkeley National Laboratory,
   One Cyclotron Road,
   Berkeley, CA 94720, USA

2. Mines ParisTech
   60, Boulevard Saint-Michel
   75 272 PARIS cedex 06

3. Institute of Electrochemical Process Engineering (IEK-3)
   Forschungszentrum Jülich GmbH
   Wilhelm-Johnen-Str.
   52428 Jülich, Germany

*corresponding author

## Keywords

Optimization, Microgrids, MILP, Battery degradation, distributed energy resources

## Highlights

- A linear model for battery degradation is proposed for MILP microgrid sizing.
- A case study of PV and storage explores the impact of considering battery aging.
- Inclusion of battery aging decreases optimal storage deployment by 6%-92%.
- For identical PV-storage systems, degradation reduces annual cost savings 5%-12%.

- Battery health constraints reduce annual battery cycling by as much as factor of 5.


# Abstract

This paper introduces a linear battery aging and degradation model to a multi-energy microgrid sizing model using mixed integer linear programming. The battery aging model and its integration into a larger microgrid sizing formulation are described. A case study is provided to explore the impact of considering battery aging on key results: optimal photovoltaic and storage capacities, optimal distributed energy resources operations strategies, and annual cost and generation metrics.

The case study results suggest that considering battery degradation in optimal microgrid sizing problems significantly impacts the perceived value of storage. Depending on capacity loss and lifetime targets, considering battery degradation is shown to decrease optimal storage capacities between 6-92% versus scenarios that do not consider battery health. When imposing constant distributed energy resource capacities, inclusion of degradation can decrease optimal annual battery cycling by as much as a factor five and reduce total annual electricity cost savings from otherwise identical photovoltaic and storage systems by 5-12%. These results emphasize that as batteries grow in maturity and ubiquity for distributed energy applications, considering battery health and capacity loss is an essential component of any analytical tool or model to guide system planning and decision-making.


# 1. Introduction

### 1.1 Microgrid design

A growing global interest in reducing environmental impacts, expanding access, and improving resiliency and reliability of energy systems is driving the integration of distributed energy resources (DER) in otherwise centralized energy networks. Microgrids, defined as clusters of interconnected loads and distributed energy resources that present themselves to the larger utility as single, flexible and controllable entities [1], [2], have emerged as an advanced solution for multi-energy DER integration, and are drawing increased interest from both academia and industry.

Due to their inherent decentralized characteristics based on local energy resources, an ability to island from the grid, and intelligent control capabilities, microgrids can contribute to more resilient, reliable, secure, cost-effective, and environmentally friendly access to energy, and can be a valuable resource to the hosting infrastructure by providing grid supportive services or deferring new investments.

However, taking full advantage of the microgrid value chain requires a diversified energy infrastructure and coordination between multiple energy vectors. Multi-energy microgrids are complex energy systems that tie together electrical, heating and cooling energy flows, and this complexity introduces significant challenges to the tasks of optimal sizing and control.

Significant efforts have been carried out to address the problem of optimal sizing in multi-energy microgrids. Among the predominant tools and methods, simulation-based and optimization-based approaches emerge as the most common. Discussions and review on different methods used in optimal microgrid sizing have been presented in [3]–[5]. Key takeaways are that simulation-based methods provide fast solutions and straightforward implementations that potentially capture non-linear behaviors in detail, but do not guarantee optimality and rely heavily on user input and prior knowledge of candidate solutions. Further, simulation methods can typically require separate algorithms to address different sizing objectives, and modeling topologies with multiple nodes may not be possible. Prominent examples of models that rely on simulation techniques are publicly available microgrid sizing tools like HOMER [6], [7] and RETSCREEN [8], or more specific initiatives, such as the study presented in [9] on the impact of lithium-ion battery operation on electricity costs, or the cost-effectiveness comparison between different battery types carried out with the ESM microgrid sizing tool presented in [10].

Conversely, optimization algorithms aim to guarantee optimality and require low user intervention to define the space of feasible solutions. These models are used for a vast array of purposes, including optimal DER investment and scheduling for minimizing annualized economic costs [11]–[14], optimal cost-effective energy storage system sizing ([15], [16]), and specific goals such as electric vehicle fleet modeling for commercial building energy management [17] and microgrid optimal design [18], or battery operation optimization for optimal PV systems management [19]. However, optimization models can become high-dimensional requiring heavy computational power and memory allocation or

become intractable. Moreover, their classification and characteristics are dictated by the nature of the formulation used, with a fundamental distinction being made with regards to linearity. Specifically, the two most common optimization approaches for DER and microgrid sizing problems are mixed integer linear programming (MILP) [11], [15]–[18] and mixed integer non-linear programming (MINLP) models. Linear and mixed integer linear models guarantee optimality and tend to solve quickly but require approximations to describe nonlinear effects. On the other hand, nonlinear and mixed integer nonlinear models may capture additional detail in nonlinear phenomena at the cost of not guaranteeing optimality, akin to simulation methods.

The Distributed Energy Resources – Customer Adoption Model (DER-CAM) [11], [17], [18] is an example of a MILP model used in multi-energy and multi-node DER and microgrid sizing. Other MILP models can be found in the literature with varying degrees of complexity, available DER, modeling accuracy, or objective function [12]–[14]. Examples for MINLP models used in multi-energy microgrid planning are also available in [20], where a genetic algorithm is applied to a resource allocation problem for energy storage systems, in [21], where evolutionary strategy is used for optimal DER sizing in microgrids, or in [20], where a multi-objective genetic algorithm is used for sizing PV-wind hybrid DC microgrids.

### 1.2 Storage modeling

The controllability requirements of a microgrid often necessitate deploying storage units in addition to generation, which provides incentives for ancillary grid services [22], or to increase self-consumption [23] up to a scenario of self-sufficiency [24].

Considering storage options in microgrid design and operation requires adequate modeling approaches: Several efforts exists to improve heat storage models ([25]–[27]) which impact the dispatch of cogeneration units. Further, a high share of renewable generation may benefit from seasonal storage where different efforts address the temporal complexity ([12], [28]–[30]).

Electric storage technologies commonly included in MILP formulations for multi-energy microgrid design rely on reservoir models [12], [14], [22], [31]–[33]. Through this approach, storage devices are typically defined by their installed capacity and the state of charge is determined by computing the

cumulative throughput due to charge and discharge operations over the time domain. In addition, reservoir models often include losses due to self discharge and constraints to limit input and output power, minimum and maximum state of charge, or impose a pre-determined calendar lifetime.

While being a proxy for battery aging, these constraints fail to capture the direct impact of charging cycles in the expected lifetime of storage, or alternatively, to impose operational limits that ensure the expected lifetime of storage is achieved given the charging cycles determined through the optimization process.

Battery aging phenomena are highly dependent on its chemical reagents and can be affected by operation conditions and surrounding environment to varying degrees. More details about the diversity of aging phenomena can be found in [34]. From a chemical standpoint, aging phenomena can be described as an array of irreversible reactions that ultimately impair the battery performance. In literature, it is most commonly defined as the decrease of battery capacity. This is the case in [35], where a Eyring equation is used to model low capacity lithium battery degradation, in [36]–[38], where empirical degradation models are designed for electric vehicles lithium-ion batteries, in [39], where an Arrhenius factor is calibrated to describe capacity fade in lithium-ion cells, or in [40], where a chemical-mechanical modeling approach is applied to lithium-ion cell degradation. In addition to capacity loss, the increase of internal resistance is often taken into account to describe aging. Examples can be found in the literature for diverse approaches such as the automated modeling of intercycle battery aging effects presented in [41], the accelerated aging tests carried out on lithium-ion batteries presented in [42], the application of the Shepherd degradation model to lead-acid batteries involved in PV systems [43], or the study presented in [44] on the dependance of lithium-ion cell aging to storage conditions. Other works propose empirical approaches by addressing the question of aging in terms of a maximum amount of charge and discharge cycles over the whole battery life [45].

Overall, two key components of battery aging are commonly distinguished: calendar aging, occuring naturally over time, as presented in [35], [37]–[39], [42] and cycle aging, determined by battery use, i.e. the cumulative battery throughput ([37], [38], [42]) or the cumulative number of charge and discharge cycles [45]. In general, calendar aging is driven by the surrounding environment conditions, notably

temperature [35], [36], [38], [39], [41], [42], [44], [46] and the battery characteristics when not in use, particularly its state of charge at rest [35], [36], [39], [44]. Conversly, and while temperature effects also occur, cycle aging is primarily driven by battery operating conditions, notably the charge and discharge rate [41], the charge and discharge current [37], [38], and the depth of discharge [41], [42], [45]. While the existing literature addressing battery aging is typically focused on small batteries or single cells, recent studies have also addressed larger sized batteries [37].

### 1.3 Objective and structure

This paper addresses the limitation found in multi-energy MILP models in considering battery aging effects by introducing a linearized formulation to account for battery aging. This formulation is introduced in the overall DER-CAM formulation and is used to derive operational constraints that guarantee meeting the expected lifetime of storage devices in multi-energy microgrid sizing problems. The objective of this paper is to develop a more accurate representation of battery costs and performance in DER investment decisions – an area of analysis where consideration of battery degradation impacts is often neglected entirely. In so doing, this paper will illustrate the importance of including use-related battery degradation impacts into holistic system optimization, which has become particularly relevant in a moment where renewable generation is reaching grid parity and storage is increasingly dominant in energy investment problems.

The remainder of this paper is organized as follows: In section 2, a simplified mathematical formulation of DER-CAM is presented, along with a discussion on the reservoir model used for electric storage and implications and requirements to incorporate battery aging. This section also presents a linearized battery aging model and its integration into the existing multi-energy microgrid sizing formulation. In section 3, a case study is introduced to demonstrate the impact of battery aging on microgrid sizing problems. The input data and assumptions of the case study exercise are provided. In Section 4 the results of the case study, related to the optimal selection and operation of DERs are discussed. Finally, Section 5 provided conclusions and the direction of future work.

# 2. Methodology

### 2.1 Proposed formulation

The Distributed Energy Resources – Customer Adoption Model (DER-CAM) is a publicly available decision support tool used for sizing and planning of decentralized multi-energy systems. This free-access tool has been developed since 2000 by the Lawrence Berkeley National Laboratory, and is formulated and implemented as a Mixed Integer Linear Program [47].

The objective of this tool is to find the DER portfolio, sizing, placement, and dispatch that optimize the site's economic and/or environmental performance against a wide array of constraints and stacked value streams. This problem is solved given hourly multi-energy loads, local weather data, cost and technical characteristics for different DER, local topology, and applicable tariffs. The tool is widely used [48] and the underlying formulation has been exhaustively peer-reviewed [49] .

In the following section a simplified DER-CAM formulation is presented. Detailed formulations are available in [22], [50], [51].

### 2.2 Reference formulation

The general DER-CAM formulation addresses a multi-energy problem where both electrical and thermal networks are considered. The objective function can be selected to either minimize total annual costs and / or environmental emissions. The cost minimization objective includes annualized costs of DER investments, DER operation and maintenance costs, power and fuel utility costs, load curtailment costs, and revenues from power exports and ancillary services market participation, as illustrated in (1).

$$\min f = \sum_{\mathrm{d}} I_{\mathrm{d}} + \sum_{\mathrm{t}} (O_{\mathrm{t}} + C_{\mathrm{t}} - X_{\mathrm{t}} - M_{\mathrm{t}}) + U \tag{1}$$

Where:

| | |
|---|---|
| D | set of DER technologies, indexed by d |
| T | set of time periods, indexed by t |
| $I_{\mathrm{d}}$ | annualized cost of investment made in technology d |
| $O_{\mathrm{t}}$ | DER operation and maintenance costs in period t |

$U$ cost of utility provided energy, power, and fuel

$C_{\mathrm{t}}$ cost associated with end-use load curtailments

$X_{\mathrm{t}}$ revenue from feed-in or net-metering power exports in period t

$M_{\mathrm{t}}$ revenue from ancillary service market participation in period t

In this simplified formulation, the annualized cost of investments $I_{\mathrm{d}}$ considers binary investment decisions, the total installed capacity of each DER, and both linear and discrete cost functions used to model different technology investments. Specifically, for DER such as PV that are commercially available in small enough modules and with economies of scale that enable the use of linear cost functions the generic form of $I_{\mathrm{d}}$ is:

$$I_{\mathrm{d}} = (b_{\mathrm{d}} * \mathrm{F_d} + P_{\mathrm{d}} * \mathrm{V_d}) * \mathrm{A_d} \quad (2)$$

Where:

$b_{\mathrm{d}}$ binary investment decision in DER d

$P_{\mathrm{d}}$ installed capacity of DER with linear cost function

$\mathrm{F_d}$ fixed investment cost in DER d

$\mathrm{V_d}$ variable investment cost in DER d

$\mathrm{A_d}$ annuity factor of DER d

For DER where these economies of scale may not be applicable, $I_{\mathrm{d}}$ takes the simpler form $I_{\mathrm{d}} = (b_{\mathrm{d}} * \mathrm{F_d}) * \mathrm{A_d}$. In this case, each discrete capacity option is indexed separately, and the installed capacity is determined by $b_{\mathrm{d}} * \mathrm{P_d}$, where $\mathrm{P_d}$ is the nameplate capacity of DER d.

The DER operation and maintenance costs $O_{\mathrm{t}}$ include fixed and variable maintenance costs, and costs of fuel required to drive conventional generators – which include costs associated with losses from conversion efficiencies as well as network losses. These are generically expressed in the form:

$$O_{\mathrm{t}} = b_{\mathrm{d}} * OMF_{\mathrm{t}}^{\mathrm{d}} + \left(g_{\mathrm{t}}^{\mathrm{d}} + o_{\mathrm{t}}^{\mathrm{d}}\right) * OMV_{\mathrm{t}}^{\mathrm{d}} \quad (3)$$

Where:

$OMF_{\mathrm{t}}^{\mathrm{d}}$ fixed O&M cost of DER d in period t

$OMV_{\mathrm{t}}^{\mathrm{d}}$ variable O&M of DER d in period t (including fuel cost)

$g_{\mathrm{t}}^{\mathrm{d}}$ total generation of DER d in period t

$o_{\mathrm{t}}^{\mathrm{d}}$ total output of storage DER d in period t

In this equation, the total generation and storage output include all possible applications, such as on-site consumption, power exports, or wholesale market participation.

Utility costs $U$ address fixed and variable costs for energy and power imports, including flat, time-of-use, hourly, and tiered tariffs. Further, utility costs also include fuel purchases for direct fuel loads (e.g. natural gas loads). Utility costs are generically described as:

$$U = \mathrm{U}^{\mathrm{F}} + \sum_{\mathrm{t}} u_{\mathrm{t}} * \mathrm{U}_{\mathrm{t}}^{\mathrm{V}} + \sum_{\mathrm{p}} \bar{u}_{\mathrm{p}} * \mathrm{U}_{\mathrm{p}}^{\mathrm{P}} \tag{4}$$

Where:

| | |
|---|---|
| $\mathrm{U}^{\mathrm{F}}$ | fixed utility cost |
| $\mathrm{U}_{\mathrm{t}}^{\mathrm{V}}$ | volumetric utility cost in period t |
| $\mathrm{U}_{\mathrm{p}}^{\mathrm{P}}$ | power demand cost in period p |
| $u_{\mathrm{t}}$ | utility import in period t |
| $\bar{u}_{\mathrm{p}}$ | peak power demand in period p |
| P | family of sets over T of power demand billing periods, indexed by p |

Revenues contemplated in this formulation include power exports associated with net-metering and feed-in programs, $S_{\mathrm{t}}$, but also those associated with the participation in ancillary service markets, $M_{\mathrm{t}}$, where both operating reserves and frequency regulation are included:

$$X_{\mathrm{t}} = \sum_{d} g_{\mathrm{t}}^{d,x} * \mathrm{X}_{\mathrm{t}}^{\mathrm{d}} \tag{5}$$

$$M_{\mathrm{t}} = \sum_{d} \left( g_{\mathrm{t}}^{d,a} + o_{\mathrm{t}}^{d,a} \right) * \mathrm{M}_{\mathrm{t}}^{\mathrm{a}} \tag{6}$$

Where:

| | |
|---|---|
| $g_{\mathrm{t}}^{d,x}$ | generation for export by DER d in period t |
| $g_{\mathrm{t}}^{d,a}$ | generation for wholesale market participation by DER d in period t |
| $o_{\mathrm{t}}^{d,a}$ | export from storage technology d for wholesale market participation in period t |
| $\mathrm{X}_{\mathrm{t}}^{\mathrm{d}}$ | power export price for DER d in period t |
| $\mathrm{M}_{\mathrm{t}}^{\mathrm{a}}$ | wholesale market clearing price in period t |

Minimizing this objective function is subject to a large set of constraints, such as energy and power balances, operational DER constraints, and financial constraints.

Energy balance constraints guarantee that energy loads are satisfied. An illustration of energy balance constraints is presented in equation (7).

$$u_t + \sum_d g_t^{d,s} + \sum_d o_t^{d,s} = l_t + i_t + c_t \quad (7)$$

Where:

| | |
|---|---|
| $g_t^{d,s}$ | on-site generation for self-consumption in period t |
| $o_t^{d,s}$ | storage output in period t |
| $l_t$ | end-use energy load in period t |
| $i_t$ | storage input in period t |
| $c_t$ | variation of end-use load in period t due to load management events |

In this equation, on-site generation includes both renewable and conventional generation, storage input and output include both contributions from conventional storage, flow batteries, or electric vehicles, and variations to end-use loads include both load increases due to load shifting events or decreases resulting from energy efficiency measures, or load curtailments.

Power balance equations are imposed to ensure current and voltage limits are observed within the microgrid topology, leading to the optimal placement of DER within the microgrid. These network constraints include estimating active and reactive power losses, and the different methods and approximations used to linearize AC power flow equations are discussed in detail in [33]. The resulting formulation is commonly described as an AC optimal power flow (AC OPF) problem with investment and sizing.

Operational constraints are used to ensure that DER operate within physical limits, that efficiency curves are respected, or that system redundancy provides resilience to contingencies, such as generator failures. When included, the additional resiliency requirements transform the formulation into a security-constrained AC OPF with investment and sizing, and formulation details are thoroughly discussed in [50].

Financial constraints are used to enforce the maximum investment payback or describe revenues and market requirements associated with participating in ancillary service markets, as described in detail in [22]. For instance, the payback constraint enforces a simple investment payback dictating that the total savings exceed investment costs over the payback period.

$$Z \geq \frac{\sum_d I'_d}{Y} \tag{8}$$

Where:

| | |
|---|---|
| Z | annual savings |
| $I'_d$ | cost of investment made in technology d |
| Y | maximum payback, in years |

### 2.3 Electric storage model

The approach used in the reference DER-CAM formulation to model conventional electric storage systems follows a reservoir model, similarly to the formulations presented in [12], [14], [31], [52]. In this approach, the capacity of electric storage devices is characterized by its energy content, and both charging and discharging decisions are used to determine the overall state of charge (energy) of the device throughout time, as described in (9).

The electric storage operation is limited by the maximum ratio of charge or discharge power to the battery's energy capacity (10, 11), and the total charge is bound by the minimum admissible charge level and the installed capacity (12). Self-discharge losses are considered in (13).

$$e_{\mathrm{t}} = e_{\mathrm{t}-1} + \eta^{\mathrm{i}} \cdot i_{\mathrm{t}} - \frac{o_{\mathrm{t}}}{\eta^{\mathrm{o}}} - \delta_{\mathrm{t}} \tag{9}$$

$$i_{\mathrm{t}} \leq E * \mathrm{i}' \tag{10}$$

$$o_{\mathrm{t}} \leq E * \mathrm{o}' \tag{11}$$

$$E * \underline{\mathrm{e}} \leq e_{\mathrm{t}} \leq E \tag{12}$$

$$\delta_{\mathrm{t}} = e_{\mathrm{t}-1} * \varphi \tag{13}$$

Where:

| | |
|---|---|
| $E$ | installed electric storage capacity |
| $e_{\mathrm{t}}$ | energy content of the electric storage at period t |
| $\mathrm{i}'$ | maximum ratio of charge power to the battery energy capacity |
| $\mathrm{o}'$ | maximum ratio of discharge power to the battery energy capacity |
| $\eta^{\mathrm{i}}$ | charging efficiency |
| $\eta^{\mathrm{o}}$ | discharging efficiency |
| $\underline{\mathrm{e}}$ | minimum state of charge of the electric storage |
| $\delta_{\mathrm{t}}$ | electric storage loss of power (self-discharge) at period t |
| $\varphi$ | self-discharge loss coefficient |

Incorporating battery aging in multi-energy microgrid sizing problems requires addressing both calendar and cycling effects. From a chemical standpoint both phenomena occur simultaneously [34], but existing modelling approaches address calendar and cycle aging independently to estimate capacity loss over time and operation. This is achieved either by considering only one of these effects to occur per time period [38], [39], by adding both components ([37], [42], [46]), or by multiplying them [35].

Calendar aging is mostly determined by time, temperature [35], [36], [38], [39], [41], [42], [44], [46] and average charging power [35], [36], [39], [44]. Cycle aging, on the other hand, tends to be driven by the total charge throughput during the life of the battery [37]–[39], [41], [42], [45], [46].

To extend the reference DER-CAM formulation and incorporate both calendar and cycle aging we consider the capacity loss model proposed in [40] and adapted in [37], based on lithium-ion battery aging behavior:

$$\mathrm{Q}^{\mathrm{T}\prime}\left(\sum_{\mathrm{t}'} Ah_{\mathrm{t}'}, \overline{\mathrm{T}'}, \mathrm{K}, \mathrm{i}^{*}\right) = (\alpha \mathrm{K}^{2} + \beta \mathrm{K} + \gamma)\varepsilon^{(\delta \mathrm{K} + \varepsilon)\,\mathrm{i}^{*}} \sum_{\mathrm{t}\prime} Ah_{\mathrm{t}\prime} + \vartheta \varepsilon^{-\frac{\mathrm{E_a}}{\mathrm{RK}}} \sqrt{\overline{\mathrm{T}'}} \tag{14}$$

Where:

| | |
|---|---|
| $\mathrm{Q}^{\mathrm{T}\prime}$ | capacity loss of electric storage during $\mathrm{T}^{\mathrm{t}}$, [%] |
| $\mathrm{T}'$ | subset of T indexed by $\mathrm{t}'$ |
| $\overline{\mathrm{T}'}$ | total duration of $\mathrm{T}'$ in days |
| $Ah_{\mathrm{t}'}$ | battery discharge in period $\mathrm{t}'$, [Ah] |
| K | surrounding temperature, [K] |
| $\mathrm{i}^{*}$ | constant charge during $\mathrm{T}'$, [Ah] |
| $\alpha, \beta, \gamma, \delta, \varepsilon$ | cycle aging coefficients, [$\mathrm{kW^{-1}K^{-2}}$], [$\mathrm{kW^{-1}K^{-1}}$], [$\mathrm{kW^{-1}}$], [$\mathrm{K^{-1}h}$], [h] |

$\vartheta, E_a, R$ calendar aging coefficients defining an Arrhenius factor, [months$^{-1/2}$], [J.mol$^{-1}$], [J.mol$^{-1}$.K$^{-1}$]

This equation describes the electric storage capacity loss as a function of cumulative discharge, elapsed time, operating temperature, and charge current. Its implementation in a MILP formulation can be achieved by linearizing the equation within specific domains. Specifically, as suggested from the work presented in [35], [40] the capacity loss can be approximated as constant for input charge values with a corresponding c-rate below 0.5, and for operating temperatures between 15 – 30 ºC or 288 – 303 ºK (Eq. 15, 16).

$$\frac{\partial Q^{T\prime}}{\partial i^*} \approx 0\,, \qquad i' \leq 0.5 \tag{15}$$

$$\frac{\partial Q^{T\prime}}{\partial K} \approx 0\,, \qquad 288 \leq K \leq 303 \tag{16}$$

Under these assumptions, the capacity loss can be estimated as a linear function of elapsed time and cumulative output. It must be noted that the average battery charge also influences calendar aging, as discussed in [35], [36], [39], [44]. However, this effect can be disregarded for standard operating temperatures, and is not considered in the models suggested in [37], [40].

Using the capacity loss estimated in (14) we can now describe storage capacity over time:

$$E_{t+\overline{T\prime}} = E_t * (1 - Q^{T'}) \tag{17}$$

Implementing this approach in the overall MILP DER-CAM formulation can be achieved by defining a target battery lifetime, $L$, and maximum capacity loss allowed during lifetime, $\overline{Q}$, to derive the linear constraint (18).

$$Q^L \leq \overline{Q} \tag{18}$$

Plugging (14) into (18) and considering the approximations discussed in (15, 16) we obtain:

$$\sum_l Ah_l \leq \frac{\overline{Q} - \vartheta \varepsilon^{-\frac{E_a}{RK}} \sqrt{L}}{(\alpha K^2 + \beta K + \gamma)\varepsilon^{(\delta K + \varepsilon)\, i\prime}} \tag{19}$$

It should be noted that the coefficients in (19) require calibration for a specific battery size. Generalizing this equation to larger storage systems consisting of multiple batteries connected in series can be achieved by defining the capacity and aging coefficients for a reference battery, $\mathrm{E^r}$, and modifying (19) accordingly:

$$\sum_{\mathrm{l}} Ah_{\mathrm{l}} \leq \frac{E}{\mathrm{E^r}} \frac{\overline{\mathrm{Q}} - \vartheta\varepsilon^{-\frac{\mathrm{E_a}}{\mathrm{RK}}}\sqrt{\mathrm{L}}}{(\alpha\mathrm{K}^2 + \beta\mathrm{K} + \gamma)\varepsilon^{(\delta\mathrm{K}+\varepsilon)\,\mathrm{i'}}} \tag{20}$$

Finally, multi-energy microgrid sizing MILP formulations such as DER-CAM typically minimize the objective function over up to one year of data [12], [14], [31], [52], which requires modifying (20) to cover the set of calculation periods T. In addition, if we multiply both terms of (20) by the battery nominal voltage we can derive a constraint (21) consistent with the reservoir model (9-13). In this constraint, we can simplify the right-hand side by introducing the term $\mathrm{N_0}(\overline{\mathrm{Q}}, \mathrm{L})$, which can be interpreted as a maximum number of cycles at maximum discharge rate that can occur during the optimization window while ensuring that the battery aging limit is not exceeded in its target lifetime. The extended MILP storage formulation based on a reservoir model and considering aging effects is then defined by (9-13) and (22).

$$\sum_{\mathrm{t}} o_{\mathrm{t}} \leq \frac{E}{\mathrm{E^r}} \frac{\mathrm{T}}{\mathrm{L}} \frac{\overline{\mathrm{Q}} - \vartheta\varepsilon^{-\frac{\mathrm{E_a}}{\mathrm{RK}}}\sqrt{\mathrm{L}}}{(\alpha\mathrm{K}^2 + \beta\mathrm{K} + \gamma)\varepsilon^{(\delta\mathrm{K}+\varepsilon)\,\mathrm{i'}}} \mathrm{V} \tag{21}$$

$$\sum_{\mathrm{t}} o_{\mathrm{t}} \leq E \cdot \mathrm{N_0}(\overline{\mathrm{Q}}, \mathrm{L}) \tag{22}$$

The maximum cycle limit $\mathrm{N_0}$ can be understood as function of the maximum tolerable capacity loss ($\overline{\mathrm{Q}}$), the target battery lifetime ($L$), the operating temperature ($K$), and the parameters used to describe the specific battery chemistry. This relationship is described in (22) and can be visualize in Figure 1. Here, the maximum number of cycles is plotted for a range of lifetimes and capacities losses for three separate operating temperatures. These values consider the lithium-ion battery parameters outlined in Table 3. As this figure indicates, the maximum allowable cycles decrease as the tolerable loss of capacity decreases, and as lifetime and operating temperatures (within the range displayed) increase. This

conforms to expectations: if greater capacity losses are allowed, the battery can be cycled more. If the expected calendar life is high or if operating temperatures are excessive, the battery must be cycled less.

# 3. Case Study

In the following section we present a case study to illustrate the impact of considering battery degradation in microgrid sizing problems. Specifically, the case study examined the impact on sizing of PV and storage, dispatch of those DER, and resulting performance metrics related to energy costs and renewable generation. The model dynamics exhibited in this case study may be impacted by the introduction of additional DERs or microgrid system complexity.

### 3.1 Load Input Data

To analyze the impact of battery aging in MILP multi-energy microgrid sizing problems we consider a hypothetical 1-bus microgrid (i.e., disregarding network constraints) in a Large Office Building in San Francisco, using prototypical end-use load data sets generated from the U.S. Department of Energy Commercial Reference Buildings [53]. This data set contains hourly load profiles including electric, heating, and cooling loads, from a range of commercial building types in multiple locations in the U.S. The key characteristics of the model used in this case study (Large Office Building in San Francisco) are presented in Table 1. Monthly electric load profile of the building model prior to DER deployment are shown in Figure 2 for each day-type modeled in DER-CAM.

### 3.2 Price Input Data

To account for both electricity and natural-gas prices we consider the E-20 and G-NR1-D electric and natural-gas tariffs in the Pacific Gas & Electric service territory, respectively. Because the DER considered in this case study address only electricity use, the results presented below will focus on costs and savings due to the electricity tariff. The E-20 electricity tariff consists of both time-dependent volumetric charges ($/kWh) and power demand charges ($/kW), whereas natural-gas prices vary only from summer to winter months, and both electric and natural-gas tariffs include a fixed monthly component, as illustrated in Table 2. In this table, the non-coincident component refers to the charge

applied to the maximum power consumption over the entire month, irrespective of the period of occurrence.

### 3.3 DER Input Data

For this case study, PV and lithium-ion battery storage devices are available (but not required) to be included in the multi-energy microgrid sizing problem. Both DER are modeled using linear cost functions, consisting of a variable (per unit of capacity purchased) component. For this analysis, PV costs are assumed to be $2500 per kW and storage costs $500 per kWh. Fixed cost components for both are assumed to be zero. DER capital costs have been selected to be generally representative of current costs, but do not correspond to specific DER products. To estimate PV generation, we assumed a conversion efficiency under test conditions of 14.9% and considered the typical meteorological year 3 (TMY3) available in the National Solar Radiation Database TMY3 data set [54] maintained by the National Renewable Energy Laboratory, using data from the San Francisco International Airport (TMY-724940). In this case study, export of excess PV is not permitted. However, it is assumed that the inverter is capable of curtailing a continuous fraction of PV generation as determined by the optimization process.

### 3.4 DER-CAM Parametric Runs

With these input data selected, DER-CAM optimizations are conducted for a range of input parameters within the new battery degradation model, to test how the results differ in comparison to a model without any representation of battery degradation. In particular, the case study is used to address how the consideration of degradation will impact:

- optimal capacities for PV and storage
- operational patterns (charging, discharging, and state-of-charge) of storage units
- energy costs savings achieved with deployed DER
- utilization of renewable generation

In total, 88 DER-CAM optimizations were conducted to capture combinations of degradation models, tolerable capacity losses, and required battery lifetimes. The results of these optimizations, and key findings related to these questions are outlined below. This investigation assumes a fixed operating

temperature of 25°C and a maximum charge rate of 0.3. While outside the scope of this case study, changes to these parameters will certainly impact results.

# 4. Results

### 4.1 Optimal DER Sizing

The first exercise within this case study is to examine the impact of the new degradation model on optimal sizing of DER. In this exercise, the optimization process is free to select any capacities of PV and storage that minimize its objective. When degradation is not considered, it is expected that storage can be overvalued, and the charging/discharging cycles generated by the optimization could adversely affect battery health if implemented under real conditions. Figure 3 shows the optimal selected storage capacity for each DER sizing run. Here, each line represents a difference tolerable capacity loss value, $\overline{Q}$, (representing the battery's end of life) along with a single, solid line indicating the no-degradation model. The x-axis shows the required lifetime, *L*, for the storage system. As expected, the no-degradation model appears to value storage more and higher capacities are selected than in any other corresponding scenario. Furthermore, as the tolerable capacity loss decreases, the optimal capacity drops, especially for values below 20%. For maximum capacity losses lower than 15% no storage capacity is included in the portfolio of investments.

As the required lifetime increases, the optimal storage capacity appears to rise moderately. The tighter charging restrictions to preserve battery life require larger storage capacities in order to capture the optimal system performance. Here it is important to note that the lifetime parameter in the no-degradation model has a substantially different meaning than in models that consider degradation. The former describes the period of time under which the battery will perform at full, nameplate capacities, while the later describes the period of time the battery must last without losing more than the tolerable capacity loss value. Consequently, a battery model considering degradation is more constrained (and thus less valuable) the longer the lifetime input (*L*), while a battery model without degradation is more valuable the longer its lifetime input.

The average optimal storage capacity selected across all lifetimes (5-12 years) in the no degradation scenario is 1208 kWh. For the degradation model with a 30% tolerable capacity loss, it is 933 kWh. For a 20% loss, it is only 618 kWh. For 10% it is zero.

The optimal PV capacities, provided in Figure 4, show a similar trend. Under the conditions analyzed, optimal PV capacity will tend to scale with optimal storage capacity. Because excess PV generation cannot be exported in this case study, additional storage is needed to shift the PV surplus to periods where it can be used to serve local loads. In cases where the perceived value of storage is high (e.g. low or no degradation), higher levels of both PV and storage are selected, because they allow for increased local generation and a reduction of utility purchases.

### 4.2 Optimal DER Operations

While the previous section explores the impact of the degradation model on DER selection, it does little to compare different DER operations, in particular storage, in response to various degradation constraints. To perform this analysis, different degradation settings are analyzed while forcing the adoption of the DER capacities determined under the no-degradation scenario onto all degradation scenarios. Thus, with DER capacities held constant across all degradation scenarios, the impact on the optimal operation can be evaluated. The optimal no-degradation capacities, which vary by storage lifetime, are given in Table 4.

Tight degradation constraints (e.g. low tolerable capacity loss or long calendar life) will restrict the frequency and magnitude of storage charging and discharging. To illustrate this effect, the hourly state-of-charge (SOC) profiles for a typical weekday for each month are plotted in Figure 5 for a subset of degradation scenarios. In each subplot, 12 monthly SOC profiles are superimposed. The opacity beneath each line indicates a likelihood of maintaining that SOC. Higher opacity indicates higher likelihood. The left column shows a relatively lax 5-year lifetime, while the right shows a relatively stricter 10-year lifetime. The no-degradation model is given in the top row; with tightening end-of-life constraints shown in subsequent rows.

Proceeding downward, as the end-of-life constraints tighten, the use of the battery decreases, as indicated by the flatter SOC profile. Charging and discharging is restricted to midday-times and often

not at all. This trend is exacerbated by the requirement of a 10-year lifetime. With a 30% end-of-life threshold, the battery is only cycled during approximately half the year. Under a 20% threshold, the battery does not appear to be cycled much at all. No results are shown for the 15% end-of-life threshold, due to infeasibility. This suggests that under the battery parameters used in this case study, even a battery that is not cycled at all will experience greater than 15% capacity loss over the 10-year period due to calendar aging alone.

### 4.3 Savings from DER

The effect of the reduced battery cycling when considering degradation will also manifest in the cost savings achievable by DER. If batteries are cycled less, there is less opportunity for price arbitrage under the TOU tariff. There is also less opportunity to absorb excess PV generation during midday periods. Finally, storage will be less available for load-flattening or peak-shaving activities, which are critical to effective demand-charge-management. Each of these will contribute to a reduction in perceived value of storage when degradation is considered.

Figure 6 andFigure 7 show the annual electricity cost savings from identical DER portfolios, separated into energy costs ($/kWh) and power demand costs ($/kW), respectively. The trends in energy cost savings (Figure 6) are very clear. As degradation impacts are increased, the same system is able to achieve diminishing levels of savings. At a certain point, (e.g. when lifetime exceeds 10 years) the degradation model can no longer find a feasible solution, and no results are shown.

The results for power demand charge savings (Figure 7) exhibit a different trend. With degradation enabled, the battery is largely used to achieve similar demand charge savings levels as the no-degradation model. However, as the degradation parameters are increased, the demand charge savings begin to drop off, indicating the battery cannot be cycled in a way to maintain the necessary amount of load flattening, without pushing the battery health outside of the permitted range. Shortly after this drop off is observed, the degradation scenarios become infeasible.

Considering only feasible cases, with the same PV and storage capacities deployed, cost savings from models that consider battery degradation lose about 6-12% of the estimated total annual cost savings compared with those estimated by the no-degradation model.

### 4.4 Resource Utilization

The impact on energy savings can be further understood by exploring the results in Figure 8. Here, annual PV curtailment fraction (i.e. the portion of total PV generation lost due to insufficient load or available storage) is shown. The trend is very clear. Increasing any of the degradation criteria increases the amount of PV that is lost, as the battery has less freedom to charge and discharge. Any lost PV generation will necessarily be replaced by utility purchases, increasing annual electricity energy costs commensurately.

Finally, the activity of the batteries themselves can be directly explored by examining the annual energy throughput (i.e. the total energy that passes through the battery each year) per unit storage installed, shown in Figure 9. Under the no-degradation model, each kWh of installed storage sees a throughput value of 293-337 kWh per year; meaning that the battery is, on average, fully cycled nearly every day. When battery degradation is considered with a tolerable capacity loss of 30% is considered, this cycle range falls to 150-325 kWh per year. When a tolerable capacity loss of 20% is considered, it falls further to 60-160 kWh per year.

These findings strongly suggest that the charging behavior exhibited by cases that do not consider degradation are generally not feasible when battery degradation and battery health are taken into account.

# 5. Conclusions

This paper discusses the introduction of a linear battery aging model in MILP DER sizing problems. A mathematical formulation of the model, and its integration into a larger multi-energy microgrid sizing problem is described. A simple case study is provided to explore the impact of key results and performance metrics of applying the new degradation model, vis-à-vis results generated by simpler reservoir storage models that do not consider degradation.

As battery technologies mature and prices fall, their attractiveness to an ever-expanding set of applications will only grow. While there are many research tools currently available, the task of optimally sizing storage resources, especially in conjunction with other DER, remains analytically

challenging and complex. Due to this complexity, model simplifications will generally always be necessary. However, as the results of the presented case study indicate, the consideration of battery degradation is an important component of system planning and will yield substantially different results in applications where storage plays a significant role.

The results of the case study explored in this paper show the perceived value of storage is highly influenced by the inclusion of degradation, as well as the parameters used to define and preserve battery health. The case study shows a decrease in optimal storage capacities between 6-92% as a result of considering degradation. Optimal cycling of the battery, as shown by annual battery throughput, can fall by as much as a factor of five. Finally, total annual electricity cost savings from otherwise identical PV and storage systems can be reduced by 5-12% based solely on the consideration of battery degradation constraints.

The results further emphasize that a failure to consider battery degradation, as well as the impact of certain charging behaviors on cumulative battery health, will likely produce recommendations that cannot be replicated in real-world DER deployments without significantly impacting durability expectations.

The work present in the paper imposed a number of assumptions that should be explored in future work. Operational temperature plays a significant role in battery health, and it is assumed to remain within favorable ranges in this work. In reality, battery cooling and ambient temperatures will affect both battery health and efficiency. Also, the parameters used in this work describe one battery chemistry at one particular point in time. Finally, only a single maximum charge rate is explored. It may be worthwhile to further explore how these parameters vary with different chemistries and incremental improvements over time.

# Acknowledgements

The Distributed Energy Resources Customer Adoption Model (DER-CAM) has been funded partly by the Office of Electricity Delivery and Energy Reliability, Distributed Energy Program of the U.S.

Department of Energy under Contract No. DE-AC02-05CH11231. DER-CAM has been designed at Lawrence Berkeley National Laboratory (LBNL) and is owned by the U.S. Department of Energy.

# References

[1] B. Lasseter, "Microgrids [distributed power generation]," *Power Eng. Soc. Winter Meet. 2001. IEEE*, vol. 1, no. C, pp. 146–149, 2001.

[2] C. Marnay, F. J. Robio, and a S. Siddiqui, "Shape of the microgrid," *Power Eng. Soc. Winter Meet. 2001. IEEE*, vol. 1, no. C, pp. 150–153 vol.1, 2001.

[3] G. Mendes, C. Ioakimidis, and P. Ferrão, "On the planning and analysis of Integrated Community Energy Systems: A review and survey of available tools," *Renewable and Sustainable Energy Reviews*, vol. 15, no. 9. pp. 4836–4854, 2011.

[4] C. Gamarra and J. M. Guerrero, "Computational optimization techniques applied to microgrids planning: A review," *Renew. Sustain. Energy Rev.*, vol. 48, pp. 413–424, 2015.

[5] a. H. Fathima and K. Palanisamy, "Optimization in microgrids with hybrid energy systems – A review," *Renew. Sustain. Energy Rev.*, vol. 45, pp. 431–446, 2015.

[6] HOMER, "Hybrid Optimization of Multiple Energy Resources." .

[7] O. Hafez and K. Bhattacharya, "Optimal planning and design of a renewable energy based supply system for microgrids," *Renew. Energy*, vol. 45, pp. 7–15, 2012.

[8] RETScreen, "Energy Management Software." .

[9] J. Neubauer and M. Simpson, "Deployment of Behind-The-Meter Energy Storage for Demand Charge Reduction," *NREL/TP-5400-63162*, p. 30, 2015.

[10] E. Hittinger, T. Wiley, J. Kluza, and J. Whitacre, "Evaluating the value of batteries in microgrid electricity systems using an improved Energy Systems Model," *Energy Convers. Manag.*, vol. 89, pp. 458–472, 2015.

[11] C. Marnay, G. Venkataramanan, M. Stadler, A. S. Siddiqui, and R. Firestone, "Optimal Technology Selection and Operation of Commercial-Building Microgrids," *IEEE Trans. Power Syst.*, vol. 23, no. 3, pp. 975–982, 2008.

[12] P. Gabrielli, M. Gazzani, E. Martelli, and M. Mazzotti, "Optimal design of multi-energy systems with seasonal storage," *Appl. Energy*, vol. 212, no. July, p. 720, 2018.

[13] H. Ren and W. Gao, "A MILP model for integrated plan and evaluation of distributed energy systems," *Appl. Energy*, vol. 87, no. 3, pp. 1001–1014, Mar. 2010.

[14] P. K. Naraharisetti, I. a. Karimi, A. Anand, and D.-Y. Lee, "A linear diversity constraint – Application to scheduling in microgrids," *Energy*, vol. 36, no. 7, pp. 4235–4243, Jul. 2011.

[15] S. X. Chen, H. B. Gooi, and M. Q. Wang, "Sizing of energy storage for microgrids," *IEEE Trans. Smart Grid*, vol. 3, no. 1, pp. 142–151, 2012.

[16] S. Bahramirad, W. Reder, and A. Khodaei, "Reliability-constrained optimal sizing of energy storage system in a microgrid," *IEEE Trans. Smart Grid*, vol. 3, no. 4, pp. 2056–2062, 2012.

[17] M. Stadler *et al.*, "Electric storage in California's commercial buildings," *Appl. Energy*, vol. 104, pp. 711–722, 2013.

[18] G. Cardoso *et al.*, "Optimal investment and scheduling of distributed energy resources with uncertainty in electric vehicle driving schedules," *Energy*, vol. 64, pp. 17–30, 2014.

[19] A. Sani Hassan, L. Cipcigan, and N. Jenkins, "Optimal battery storage operation for PV systems with tariff incentives," *Appl. Energy*, vol. 203, pp. 422–441, 2017.

[20] M. B. Shadmand and R. S. Balog, "Multi-objective optimization and design of photovoltaic-wind hybrid system for community smart DC microgrid," *IEEE Trans. Smart Grid*, vol. 5, no. 5, pp. 2635–2643, 2014.

[21] T. Logenthiran, D. Srinivasan, a. M. Khambadkone, and T. Sundar Raj, "Optimal sizing of Distributed Energy Resources for integrated microgrids using Evolutionary Strategy," *2012 IEEE Congr. Evol. Comput.*, pp. 1–8, 2012.

[22] G. Cardoso, M. Stadler, S. Mashayekh, and E. Hartvigsson, "The impact of ancillary services in optimal DER investment decisions," *Energy*, vol. 130, pp. 99–112, 2017.

[23] F. M. Vieira, P. S. Moura, and A. T. de Almeida, "Energy storage system for self-consumption of photovoltaic energy in residential zero energy buildings," *Renew. Energy*, vol. 103, pp. 308–320, 2017.

[24] R. Khalilpour and A. Vassallo, "Leaving the grid: An ambition or a real choice?," *Energy Policy*, vol. 82, no. 1, pp. 207–221, 2015.

[25] D. Steen, M. Stadler, G. Cardoso, M. Groissböck, N. DeForest, and C. Marnay, "Modeling of thermal storage systems in MILP distributed energy resource models," *Appl. Energy*, vol. 137, pp. 782–792, 2015.

[26] H. Wang, W. Yin, E. Abdollahi, R. Lahdelma, and W. Jiao, "Modelling and optimization of CHP based district heating system with renewable energy production and energy storage," *Appl. Energy*, vol. 159, pp. 401–421, 2015.

[27] H. Harb, J. N. Paprott, P. Matthes, T. Schütz, R. Streblow, and D. Müller, "Decentralized scheduling strategy of heating systems for balancing the residual load," *Build. Environ.*, vol. 86, pp. 132–140, 2015.

[28] S. Samsatli and N. J. Samsatli, "A general spatio-temporal model of energy systems with a detailed account of transport and storage," *Comput. Chem. Eng.*, vol. 80, pp. 155–176, 2015.

[29] R. Renaldi and D. Friedrich, "Multiple time grids in operational optimisation of energy systems with short- and long-term thermal energy storage," *Energy*, vol. 133, pp. 784–795, 2017.

[30] L. Kotzur, P. Markewitz, M. Robinius, and D. Stolten, "Time series aggregation for energy system design: Modeling seasonal storage," *Appl. Energy*, vol. 213, no. October 2017, pp. 123–135, 2018.

[31] H. Ren and W. Gao, "A MILP model for integrated plan and evaluation of distributed energy systems," *Appl. Energy*, 2010.

[32] T. Schittekatte, M. Stadler, G. Cardoso, S. Mashayekh, and N. Sankar, "The impact of short-term stochastic variability in solar irradiance on optimal microgrid design," *IEEE Trans. Smart Grid*, vol. 3053, no. c, pp. 1–9, 2016.

[33] S. Mashayekh, M. Stadler, G. Cardoso, and M. Heleno, "A mixed integer linear programming approach for optimal DER portfolio, sizing, and placement in multi-energy microgrids," *Appl. Energy*, vol. 187, pp. 154–168, 2017.

[34] M. R. Palacin and A. de Guibert, "Why do batteries fail?," *Science (80-. ).*, vol. 351, no. 6273, pp. 1253292–1253292, 2016.

[35] P. Gyan, I. Baghdadi, O. Briat, and J. Del, "Lithium battery aging model based on Dakin ' s degradation approach," *J. Power Sources*, vol. 325, pp. 273–285, 2016.

[36] A. Cordoba-Arenas, S. Onori, Y. Guezennec, and G. Rizzoni, "Capacity and power fade cycle-life model for plug-in hybrid electric vehicle lithium-ion battery cells," *J. Power Sources*, vol. 278, pp. 473–483, 2015.

[37] D. Wang, J. Coignard, T. Zeng, C. Zhang, and S. Saxena, "Quantifying electric vehicle battery degradation from driving vs. vehicle-to-grid services," *J. Power Sources*, vol. 332, pp. 193–203, 2016.

[38] M. Petit, E. Prada, and V. Sauvant-Moynot, "Development of an empirical aging model for Li-ion batteries and application to assess the impact of Vehicle-to-Grid strategies on battery lifetime," *Appl. Energy*, vol. 172, pp. 398–407, 2016.

[39] E. Redondo-iglesias *et al.*, "Modélisation du vieillissement calendaire de cellules lithium-ion ( graphite / LiFePO4 ) avec prise en compte de la dérive de leur état de charge .," no. Sge, pp. 7–9, 2016.

[40] J. Purewal, J. Wang, J. Graetz, S. Soukiazian, H. Tataria, and M. W. Verbrugge, "Degradation of lithium ion batteries employing graphite negatives and nickel-cobalt-manganese oxide + spinel manganese oxide positives: Part 2, chemical-mechanical degradation model," *J. Power Sources*, vol. 272, pp. 1154–1161, 2014.

[41] M. Petricca, D. Shin, A. Bocca, A. Macii, E. Macii, and M. Poncino, "Automated generation of battery aging models from datasheets," *2014 32nd IEEE Int. Conf. Comput. Des. ICCD 2014*, pp. 483–488, 2014.

[42] J. Schmalstieg, S. Käbitz, M. Ecker, and D. U. Sauer, "From Accelerated Aging Tests to a Lifetime Prediction Model : Analyzing Lithium-Ion Batteries," *27th World Electr. Veh. Symp. Exhib. EVS 2014; Barcelona; Spain*, pp. 1–12, 2014.

[43] A. Cherif, M. Jraidi, and A. Dhouib, "A battery ageing model used in stand alone PV systems," *J. Power Sources*, vol. 112, no. 1, pp. 49–53, 2002.

[44] L. . Su *et al.*, "Path dependence of lithium ion cells aging under storage conditions," *J. Power Sources*, vol. 315, pp. 35–46, 2016.

[45] A. Bocca, A. Sassone, D. Shin, A. Macii, E. Macii, and M. Poncino, "An equation-based battery cycle life model for various battery chemistries," *IEEE/IFIP Int. Conf. VLSI Syst. VLSI-SoC*, vol. 2015–Octob, pp. 57–62, 2015.

[46] J. Purewal, J. Wang, J. Graetz, S. Soukiazian, H. Tataria, and M. W. Verbrugge, "Degradation of lithium ion batteries employing graphite negatives and nickel-cobalt-manganese oxide + spinel manganese oxide positives: Part 2, chemical-mechanical degradation model," *J. Power Sources*, vol. 272, pp. 1154–1161, 2014.

[47] LBNL, "DER-CAM Website." .

[48] LBNL, "DER-CAM Users and Partners." .

[49] LBNL, "DER-CAM Publications." .

[50] S. Mashayekh *et al.*, "Security-Constrained Design of Isolated Multi-Energy Microgrids," *IEEE Trans. Power Syst.*, vol. 8950, no. c, pp. 1–1, 2017.

[51] S. Mashayekh, M. Stadler, G. Cardoso, and M. Heleno, "A mixed integer linear programming approach for optimal DER portfolio, sizing, and placement in multi-energy microgrids," *Appl. Energy*, vol. 187, 2017.

[52] D. Henning, S. Amiri, and K. Holmgren, "Modelling and optimisation of electricity, steam and district heating production for a local Swedish utility," *Eur. J. Oper. Res.*, vol. 175, no. 2, pp. 1224–1247, 2006.

[53] U.S. Department of Energy, "Commercial Reference Buildings." .

[54] N. R. E. Laboratory, "National Solar Radiation Data Base - 1991- 2005 Update: Typical Meteorological Year 3." .

# Figures

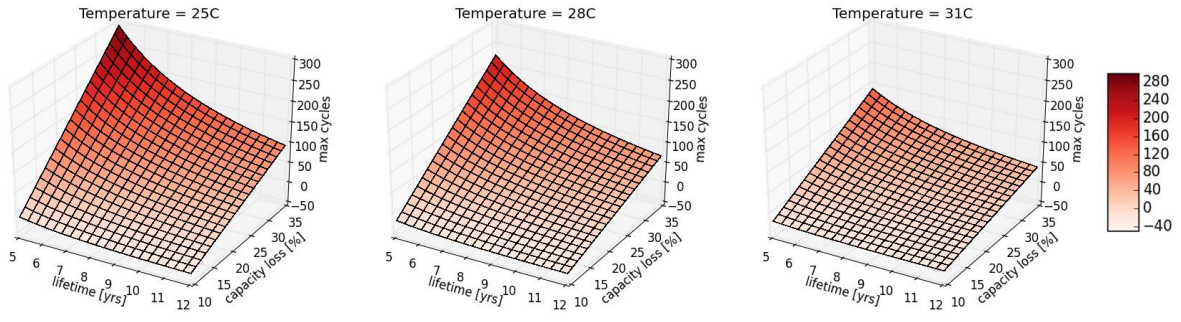


***Figure 1. Maximum annual charging cycles ($N_0$) at maximum charge rates for various degradation model parameters: battery lifetime, maximum tolerable capacity loss, and operating temperature***

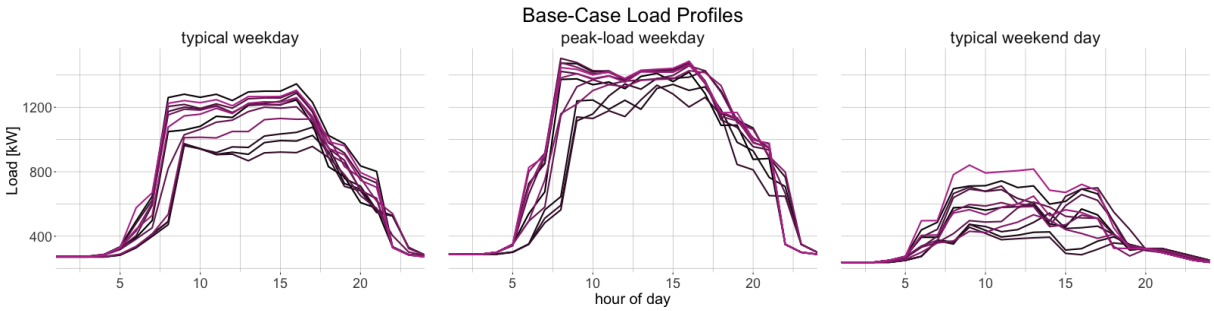


***Figure 2. Monthly load profiles by day-type for base-case scenario without DER deployment.***

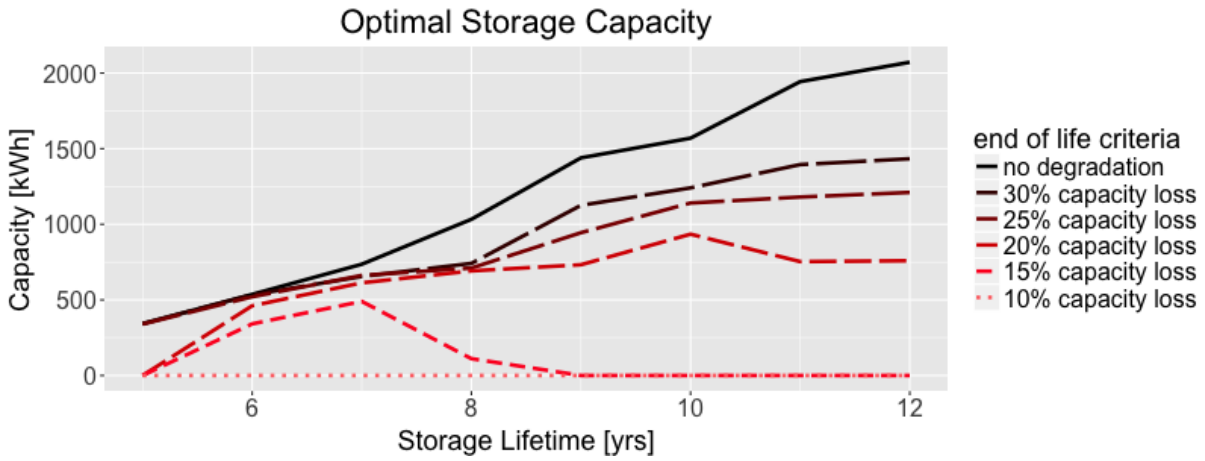


***Figure 3. Optimal storage capacities under different battery degradation models***

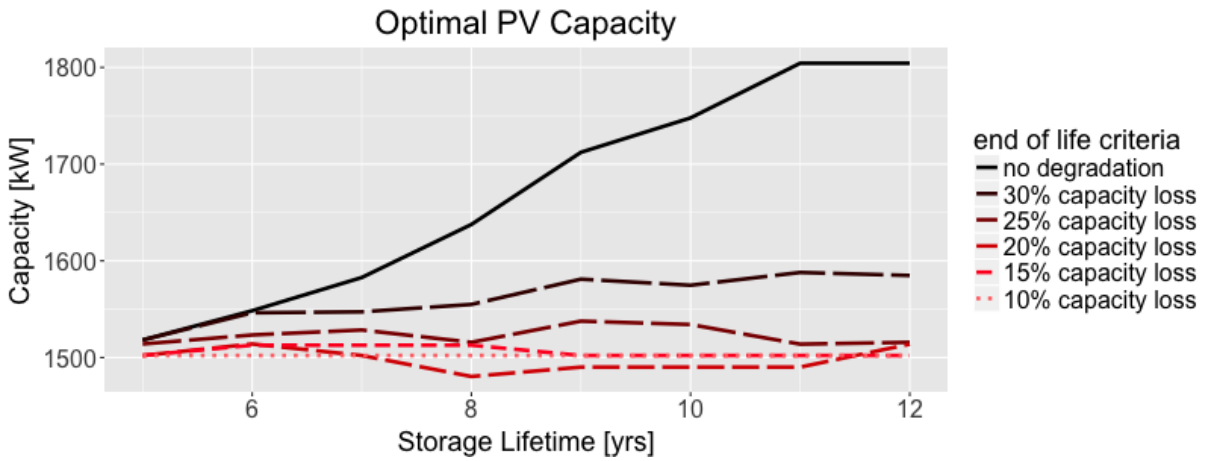


***Figure 4. Optimal PV capacities under different battery degradation models***

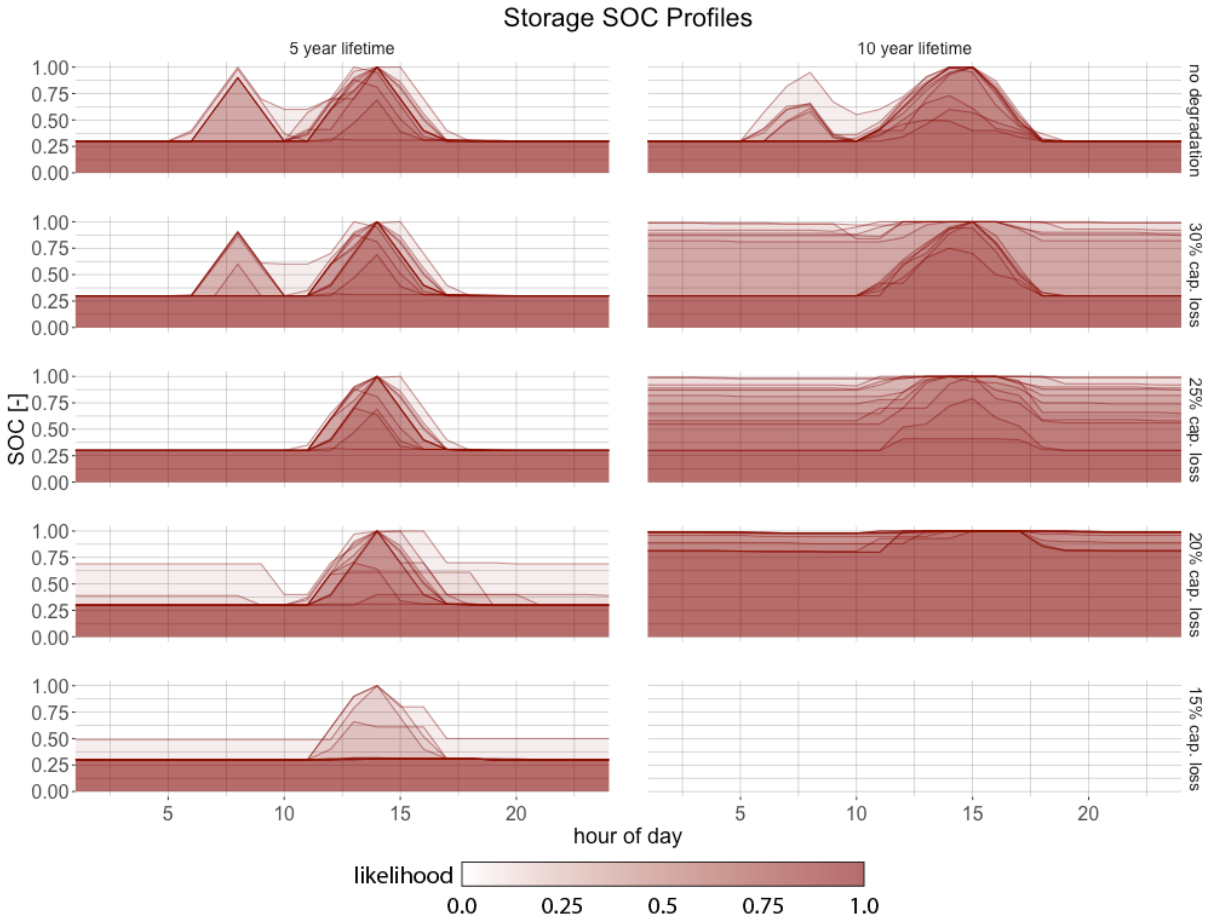


***Figure 5. The optimal weekday profiles for storage state-of-charge (SOC) across all months indicate the frequency and depth of discharge under each degradation scenario. Each subplot superimposes 12 monthly SOC profiles. The opacity of each profile indicates the likelihood of maintaining a high or low SOC at each hour throughout the year. Higher opacity indicates higher likelihood. Note: missing data indicate infeasible degradation limits.***

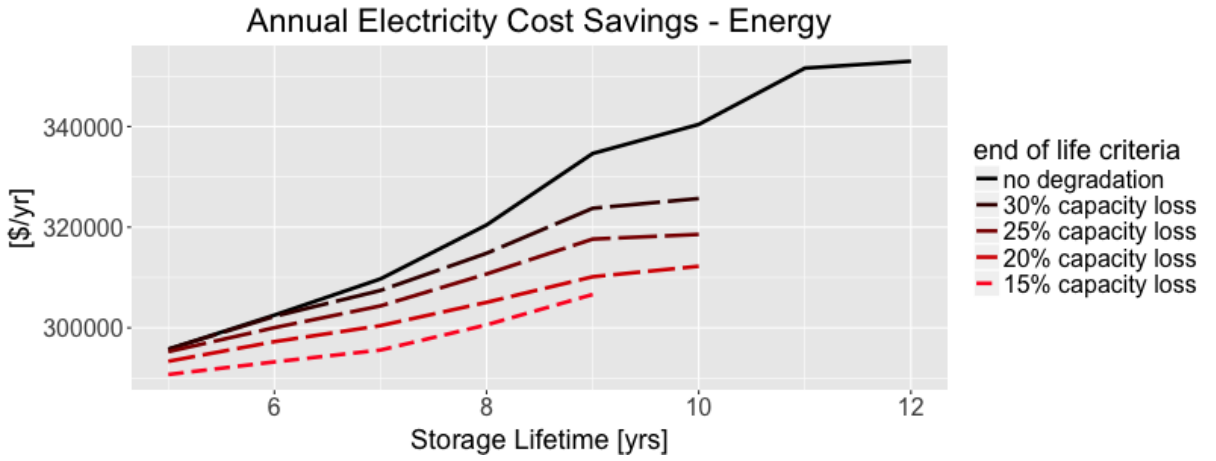

***Figure 6. Annual costs savings from electricity energy charges with fixed DER capacities. Note: missing values indicate infeasible configurations***

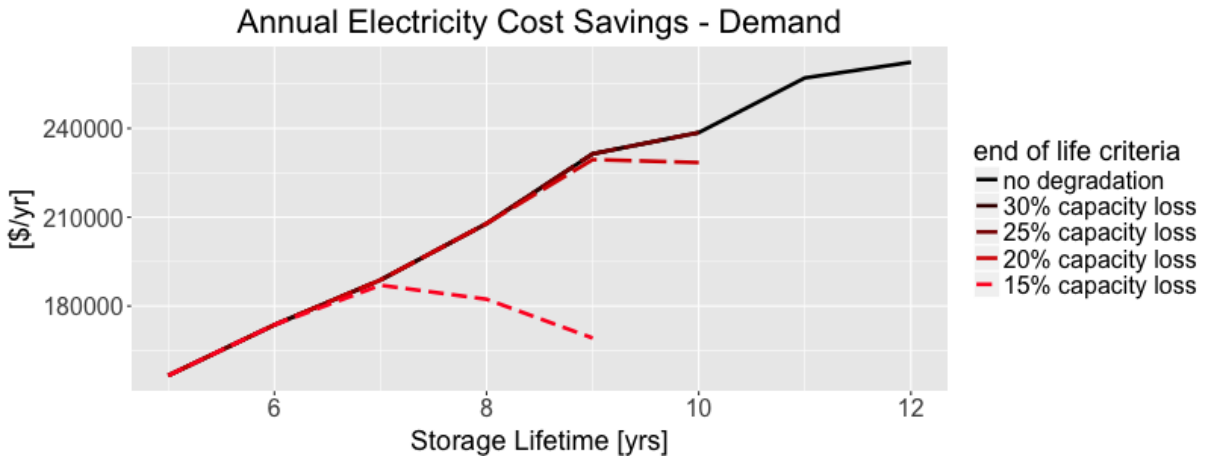


***Figure 7. Annual costs savings from electricity demand charges with fixed DER capacities. Note: missing values indicate infeasible configurations.***

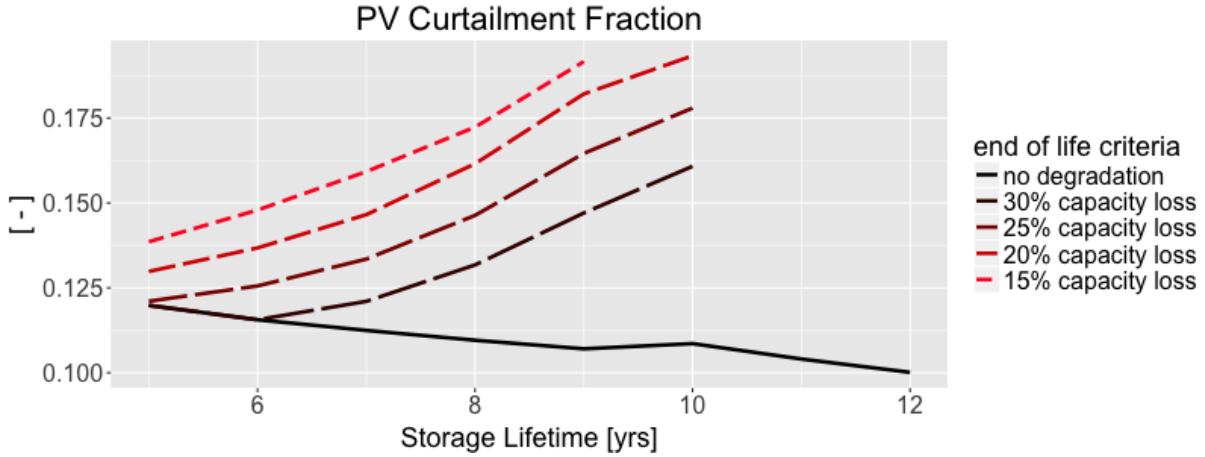


***Figure 8. Fraction of annual PV generation curtailed under various degradation model scenarios. Note: missing values indicate infeasible configurations.***

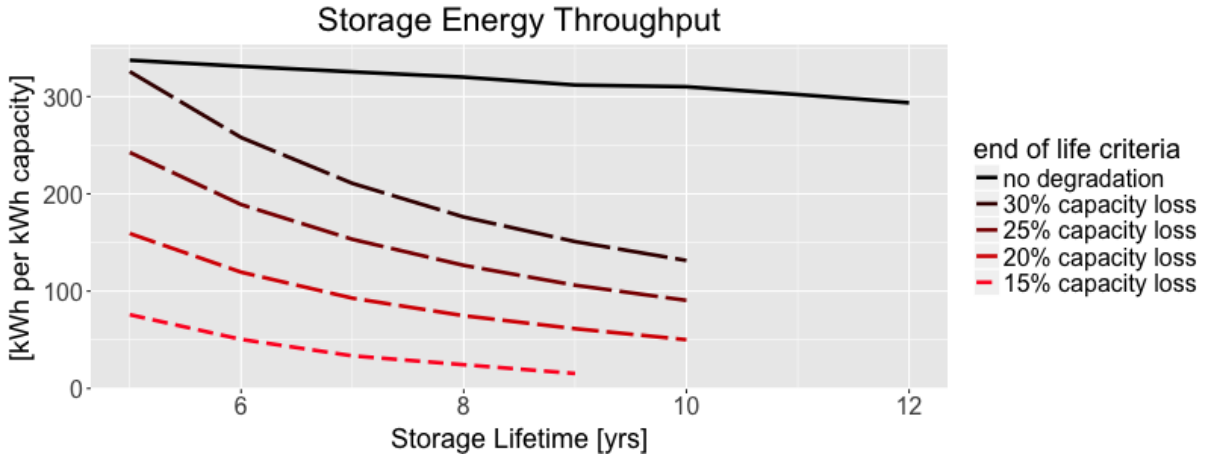

***Figure 9. Annual energy throughput (per kWh of installed storage capacity) under various degradation model scenarios. Note: missing values indicate infeasible configurations.***

# Tables

***Table 1 – Large Office Building in San Francisco***

| Building Type | Floor Area ($ft^2$) | Floors | Max. electric demand [kW] | Total electric demand [MWh] | Max. daily nat-gas demand [kWh] | Total gas demand [MWh] |
|---|---|---|---|---|---|---|
| Large Office | 498,588 | 12 | 1,504 | 5,734 | 3,011 | 540 |

***Table 2 - PG&E tariffs E-20 and G-NR1-D***

| season | E-20-D | | | | | | | G-NR1-D |
|---|---|---|---|---|---|---|---|---|
| | Fixed monthly fee: $1182.57 | | | | | | | $49.9 |
| | off-peak | | mid-peak | | peak | | non-coin | natural-gas |
| | $/kWh | $/kW | $/kWh | $/kW | $/kWh | $/kW | $/kW | $/kWh |
| winter | 0.083 | - | 0.096 | 0.05 | - | - | 16.89 | 0.0374 |
| summer | 0.076 | - | 0.101 | 5.05 | 0.138 | 18.14 | 16.89 | 0.0336 |
| seasons: summer May-Oct; winter Nov-Apr<br>summer off-peak: all weekend and week days 9pm – 8am; mid-peak: 8am – 12pm and 6pm – 9pm; peak: 12pm – 6pm<br>winter off-peak: all weekend and week days 9pm – 8 am; mid-peak: 8am – 9pm | | | | | | | | |

***Table 3 – Summary of battery chemistry parameters used to test application of degradation model***

| Parameter | Value | unit |
|---|---|---|
| $\alpha$ | 5.04e-6 | $kW^{-1}K^{-2}$ |
| $\beta$ | -2.998e-3 | $kW^{-1}K^{-1}$ |
| $\gamma$ | 0.446 | $kW^{-1}$ |
| $\delta$ | -6.7e-3 | $K^{-1}h$ |
| $\varepsilon$ | 2.35 | h |
| $\upsilon$ | 4944 | $months^{-1/2}$ |
| Ea | 24500 | $J.mol^{-1}$ |
| R | 8.314 | $J.mol^{-1}.K^{-1}$ |
| i’ | 0.3 | - |
| T | 298 | K |

***Table 4 – Optimal DER capacities from no-degradation model by given battery lifetime***

| storage lifetime [years] | 5 | 6 | 7 | 8 | 9 | 10 | 11 | 12 |
|---|---|---|---|---|---|---|---|---|
| PV capacity [kW] | 1518 | 1548 | 1583 | 1638 | 1712 | 1748 | 1804 | 1804 |
| storage capacity [kWh] | 342 | 536 | 736 | 1033 | 1439 | 1570 | 1943 | 2072 |